SIAM J. Applied Dynamical Systems
Vol. 7, No. 1, pp. 186–206


# Localized Pattern Formation with a Large-Scale Mode: Slanted Snaking*

J. H. P. Dawes†

**Abstract.** Steady states of localized activity appear naturally in uniformly driven, dissipative systems as a result of subcritical instabilities. In the usual setting of an infinite domain, branches of such localized states bifurcate at the subcritical "pattern-forming" instability and intertwine in a manner often referred to as "homoclinic snaking." In this paper we consider an extension of this paradigm where, in addition to the pattern-forming instability (with nonzero wavenumber), a large-scale neutral mode exists, having zero growth rate at zero wavenumber. Such a situation naturally arises in the presence of a conservation law; we give examples of physical systems in which this arises, in particular, thermal convection in a horizontal fluid layer with a vertical magnetic field. We introduce a novel scaling that allows the derivation of a nonlocal Ginzburg–Landau equation to describe the formation of localized states. Our results show that the existence of the large-scale mode substantially enlarges the region of parameter space where localized states exist and are stable.

**Key words.** homoclinic snaking, pattern formation, bifurcation

**AMS subject classifications.** 76E25, 34E13, 35B32

**DOI.** 10.1137/06067794X

## 1. Introduction.

Recent decades have seen a sustained level of interest in systems whose response is spatially localized despite a spatially uniform applied forcing. One broad class of systems which display such localized states of activity is both driven and strongly dissipative, and displays "pattern-forming" (also called Turing) instabilities at which spatially homogeneous solutions become unstable and spatial structure appears [11, 19, 25]. It is widely appreciated that, while supercritical pattern-forming instabilities lead to spatially extended (and almost periodic) structures, subcritical instabilities robustly lead to localized patterns [21, 37, 8, 30, 5]. Localized steady-state pattern formation has been observed in a huge variety of experiments and models for physical, chemical, and biological systems, for example, neural dynamics [23], elastic buckling [20], and nonlinear optics [1, 35]. In other cases, for example, vertically vibrated granular media [34], the localized pattern is oscillatory in nature. In many problems the existence of the localized states can be heuristically explained by an energetic argument: at a critical parameter value, often called the "Maxwell point," the system has no energetic preference between the "ground state," corresponding to no pattern, and the patterned state. Once a localized state has been formed there is a locking between the phase of the pattern and the phase of the envelope which allows the localized state to persist over a finite range of parameter values, as first remarked on by Pomeau [26].

*Received by the editors December 18, 2006; accepted for publication (in revised form) by M. Silber November 2, 2007; published electronically February 8, 2008. This research was supported by Newnham College, Cambridge, and by the Royal Society.
http://www.siam.org/journals/siads/7-1/67794.html
†DAMTP, Centre for Mathematical Sciences, University of Cambridge, Wilberforce Road, Cambridge, CB3 0WA, UK (j.h.p.dawes@damtp.cam.ac.uk).

Mathematically, much has been done to investigate canonical model problems displaying subcritical pattern-forming instabilities and therefore localized patterns. One such model equation is the one-dimensional Swift–Hohenberg equation

$$w_t = [r - (1 + \partial_{xx}^2)^2]w + N(w) \tag{1.1}$$

(writing $\partial_{xx}^2$ as a convenient abbreviation for $\partial^2/\partial x^2$), which has been studied in detail in the particular cases $N(w) = sw^2 - w^3$ and $N(w) = sw^3 - w^5$, where $s > 0$ controls the subcritical nature of the pattern-forming instability. These choices for $N(w)$ are commonly referred to as the "quadratic-cubic" and "cubic-quintic" cases, respectively. Careful investigations of these localized states have been carried out by several authors including Sakaguchi and Brand [30] and Burke and Knobloch [5]. Many different localized and front-like solutions between steady states have been reported. For our present purposes, we note that the most obvious consequence of a subcritical bifurcation is the existence of stable localized states in a small subregion between the linear instability of the state $w(x,t) \equiv 0$ at $r = 0$ and the saddle-node bifurcation at $r = r_{sn} < 0$ on the primary branch of uniform amplitude pattern. The width of this region is exponentially small in the small amplitude parameter $\varepsilon$ employed in the standard Ginzburg–Landau multiple-scales expansion near $r = 0$ [22]. Moreover, since the usual "spatial dynamics" analysis assumes an infinitely wide domain $-\infty < x < \infty$, localized states containing arbitrary numbers of pattern bumps are simultaneously stable over almost all of this region.

Concentrating on the cubic-quintic case, a final widely appreciated, and well-understood, point is that two distinct pairs of branches of localized states persist over the locking region. One pair corresponds to locking at relative phases of $\phi = 0$ and $\phi = \pi$ (these are related by the $w \to -w$ symmetry present in the cubic-quintic case) and the other pair to the relative phases $\phi = \pi/2$ and $\phi = -\pi/2$, similarly related by symmetry. The first pair corresponds to localized states that are even about the midpoint, and the second pair corresponds to states that are odd about the midpoint. This robust phase-locking is exactly the "locking" intuitively understood by Pomeau.

Intriguingly, the spatial dynamics analysis shows that these branches of localized states, that generically bifurcate from $r = 0$, exist in $r < 0$ down to saddle-node bifurcations slightly below the Maxwell point. They then undergo a sequence of repeated and intertwined saddle-node bifurcations on alternate sides of the Maxwell point; after each pair of saddle-node bifurcations the localized state gains an extra pair of bumps. In a finite domain the branches terminate in bifurcations from the uniform amplitude pattern located near $r = 0$ and near the saddle-node bifurcation at $r = r_{sn}$. In an infinite domain the process of saddle-node bifurcations and gaining extra bumps continues ad infinitum. This sequence of repeated saddle-node bifurcations in an infinite domain is known as "homoclinic snaking" since all the states approach $w = 0$ as $x \to \pm\infty$. A brief explanation of the "homoclinic snaking" phenomenon is that at some parameter value $r = r_{mx}$, $r_{sn} < r_{mx} < 0$, there exists a "Maxwell point" where there exists a stationary front between the trivial solution $w = 0$ and the uniform spatially periodic pattern. In the corresponding spatial dynamical system this heteroclinic connection becomes a heteroclinic tangle when normal form symmetry is broken. Within the heteroclinic tangle we can identify intersections of the stable and unstable manifolds of $w = 0$;

these correspond to spatial homoclinic orbits that comprise the "homoclinic snaking" and they can be shown to persist near $r = r_{mx}$, rather than existing only exactly at $r = r_{mx}$.

In a large but finite domain (with periodic boundary conditions), it appears that localized states persist and continue to exhibit intertwined wiggles around the Maxwell point [18]. In a finite domain they are not truly "localized" since the domain is bounded, but they clearly converge to the infinite domain solutions as the domain size $L \to \infty$. A detailed discussion of persistence and the evolution of the bifurcation structure with domain size will be presented elsewhere.

In this paper we consider a class of pattern-forming systems that differs from (1.1) in a fundamental way; a neutrally stable long-wavelength mode exists in addition to the pattern-forming instability at wavenumber $k = 1$. Our broad motivation comes from three physical situations: thermal convection in the presence of a vertical magnetic field [13, 10], vertically vibrated granular media [17, 34], and thin films [16]. In all three cases the large-scale mode arises due to the existence of a conserved quantity in the dynamics. In magnetoconvection this is the total flux of magnetic field through the fluid layer; in the granular and thin film cases the conserved quantity is the total mass. We remark that such a conserved quantity makes sense only for *finite* experimental domains, and our analysis takes this into account.

The treatment of the large-scale mode in magnetoconvection differs in one respect from the granular media and thin film cases; in the former problem the large-scale mode (the horizontally averaged vertical component of the magnetic field) can take either sign; the dynamics is unchanged by this, so the dynamical equations must also remain unchanged. In the latter two cases the large-scale mode quantity is a scalar, density-like, quantity and no sign-change symmetry exists. We focus in this paper on the symmetric case relevant to magnetoconvection; the density-like case is very similar and we summarize a few calculations in an appendix. As we will show, the presence of a large-scale mode stretches the snaking behavior out over a substantial region of parameter space and enables localized states to exist both below the saddle-node bifurcation on the subcritical uniform amplitude branch at $r = r_{sn}$ and far above the point of linear instability of the trivial state.

Pattern formation in the presence of a long-wavelength neutral mode of this kind was considered by Matthews and Cox [24], who carried out a weakly nonlinear analysis of a Swift–Hohenberg-type equation modified by applying $\partial^2_{xx}$ to the right-hand side of (1.1) to produce a dispersion relation that tended to zero (i.e., indicated neutral stability) as $k \to 0$. These authors considered the pattern amplitude to be $O(\varepsilon)$ and the large-scale mode to deviate by only an $O(\varepsilon^2)$ amount from the initially homogeneous state. While asymptotically correct, these scalings are unable to capture solutions where the fluctuations in the large-scale mode are large. As a result, numerical solutions often blow up, and higher-order stabilizing terms were found to be required [10]. Similar difficulties were noted by Golovin, Davis, and Voorhees [16].

In this paper we present a modified multiple-scales analysis that uses the diffusivity of the large-scale mode as the small parameter. We show that this enables the asymptotics for small-amplitude patterns to nevertheless capture the effect of $O(1)$ fluctuations in the large-scale mode. In consequence, this asymptotic treatment avoids the singularities found by earlier authors. The layout of the paper is as follows. Section 2 proposes the extension of (1.1) which we study; details linking it directly to the governing equations for magnetoconvection are deferred to Appendix A. Appendix B summarizes the multiple-scales derivation in the very

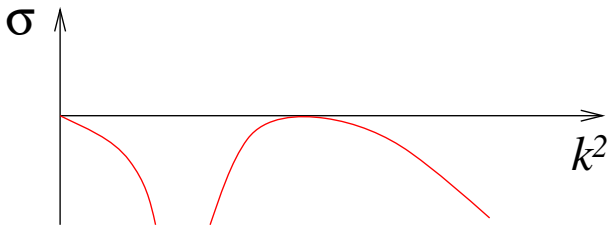


**Figure 1.** *Sketch of the growth rate $\sigma(k^2)$ for a reflection-symmetric pattern-forming instability at wavenumber $k = 1$, in the presence of a large-scale mode that is neutrally stable as $k \to 0$.*

similar case of a density-like large-scale mode, appropriate to the vibrated granular medium and thin film cases. In section 3 we return to the Swift–Hohenberg ansatz and compare the results of the multiple-scales approach with results from numerical continuation. Section 4 concludes the paper.

## 2. Ginzburg–Landau asymptotics.

In this section we propose a model equation for pattern formation coupled to a large-scale mode, appropriate for magnetoconvection. We assume that the pattern-forming domain $0 \le x \le L$ is large, but, crucially, finite, and we carry out a multiple-scales analysis to derive an amplitude equation similar to the Ginzburg–Landau equation, but containing a nonlocal term, which captures the influence of the large-scale mode. From the Ginzburg–Landau equation we deduce the existence of modulational instabilities that lead to localized states and investigate scaling laws governing the location of the bifurcation points.

### 2.1. Model equations.

Suppose that a one-dimensional pattern-forming system is described by the pattern amplitude $w(x,t)$ and the large-scale mode $B(x,t)$. We consider the dispersion curves of the linearized growth rate as a function of perturbation wavenumber $k$ to take the form shown in Figure 1, with quadratic maxima at $k = 0$ and $k = 1$.

We further assume that the system is translationally invariant and reflection-symmetric (i.e., $x \to -x$). Hence a conservation law for $B(x,t)$ contains only even numbers of derivatives. In the absence of the large-scale mode we assume that the pattern-forming instability is supercritical; this is appropriate for thermal convection. An additional symmetry requirement is appropriate for magnetoconvection: that the dynamics is invariant under a change in the sign of the large-scale mode $B(x,t)$. Model equations constrained to have these properties are

$$w_t = [r - (1 + \partial_{xx}^2)^2]w - w^3 - QB^2 w, \tag{2.1}$$

$$B_t = \varepsilon B_{xx} + \frac{c}{\varepsilon}(Bw^2)_{xx}, \tag{2.2}$$

where natural (and analytically tractable) forms of the coupling terms with coefficients $Q$ and $c/\varepsilon$ have been taken. The factor of $\varepsilon^{-1}$ in the second equation enables an asymptotic balance between the nonlinear and the diffusion terms to occur when the pattern amplitude $w(x,t)$ is $O(\varepsilon)$. As shown in Appendix B, this factor of $\varepsilon^{-1}$ appears naturally in magnetoconvection.

Integrating (2.2) over the domain $0 \le x \le L$ and applying periodic boundary conditions imply that $\frac{1}{L}\int_0^L B(x,t)dx \equiv \langle B \rangle$ is constant in time; by rescaling $B(x,t)$ we may take it to be

unity. Essentially, this rescaling absorbs the original mean value $\langle B\rangle$ into the coupling parameter $Q$. Such a rescaling corresponds exactly to the usual nondimensionalization employed in magnetoconvection, where $Q$ is known as the Chandrasekhar number [7, 27].

We now restrict our attention to steady solutions, setting $\partial_t \equiv 0$, and integrating (2.2) twice to obtain

$$B = \frac{P}{1+cw^2/\varepsilon^2}, \tag{2.3}$$

where $P$ is a constant of integration that corresponds to the value of the large-scale mode away from the localized pattern. Using $\langle B\rangle = 1$ we can now compute $P$ as an integral over the domain; $P$ therefore becomes a nonlocal functional of the pattern amplitude $w(x)$:

$$\frac{1}{P} = \left\langle \frac{1}{1+cw^2/\varepsilon^2} \right\rangle. \tag{2.4}$$

Substituting into (2.1) and looking for steady states, we obtain the nonlocal Swift–Hohenberg equation

$$0 = [r-(1+\partial_{xx}^2)^2]w - w^3 - \frac{QP^2w}{(1+cw^2/\varepsilon^2)^2}. \tag{2.5}$$

The study of bifurcations and solution stability in nonlocal equations is an area of substantial current interest; see, for example, [4, 12] and the references therein. In this paper such difficulties are largely bypassed since, although (2.5) is nonlocal, the linear stability analysis of $w(x) \equiv 0$ remains a local problem. As a result, the usual approaches to small-amplitude solutions of the Swift–Hohenberg equation can be applied, as we now show.

We now introduce the multiple-scales ansatz

$$w(x,t) = \varepsilon A(X)\sin x + \varepsilon^2 w_2 + \varepsilon^3 w_3 + \cdots, \tag{2.6}$$

defining the long lengthscale $X = \varepsilon x$. We rescale the parameters $r = \varepsilon^2\mu$ and $Q = \varepsilon^2 q$ since we are focusing on small-amplitude patterns. The amplitude $A(X)$ can be taken to be real since the instability which generates localized states occurs in the pattern amplitude and not in its phase. At third order in the expansion an amplitude equation for $A(X)$ is obtained by multiplying by $\sin x$ and integrating over the short lengthscale, denoting the average as $\frac{1}{2\pi}\int_0^{2\pi} f(x)dx \equiv \langle f(x)\rangle_x$. We obtain

$$0 = \mu A + 4A_{XX} - 3A^3 - 2qP^2\left\langle \frac{A\sin^2 x}{(1+cA^2\sin^2 x)^2}\right\rangle_x, \tag{2.7}$$

where $P$ now becomes

$$\begin{aligned}\frac{1}{P} &= \frac{1}{\varepsilon L}\int_0^{\varepsilon L}\frac{1}{2\pi}\int_0^{2\pi}\frac{1}{1+cA^2\sin^2 x}\,dx\,dX \\ &\equiv \left\langle \left\langle \frac{1}{1+cA^2\sin^2 x}\right\rangle_x\right\rangle_X = \left\langle \frac{1}{\sqrt{1+cA^2}}\right\rangle_X.\end{aligned} \tag{2.8}$$

Carrying out the $x$-integral in (2.7), we obtain

$$0 = \mu A + 4A_{XX} - 3A^3 - \frac{qP^2A}{(1+cA^2)^{3/2}}. \tag{2.9}$$

It follows that the trivial state $A(X) \equiv 0$ (for which $B = 1$) undergoes a pitchfork bifurcation at $\mu = q$. The pitchfork bifurcation is supercritical for small $q$ but becomes subcritical for $cq > 6$, as can be checked by expanding both the nonlinear term and $P$ for small $A$ in (2.9).

**2.2. Modulational instabilities.** As is typical in subcritical bifurcations of this kind, secondary bifurcations occur close to $\mu = 0$, and close to the saddle-node point on the uniform branch, which results in localized states. Interestingly, for this problem these secondary modulational instabilities exist also for $2 < cq < 6$ where the primary bifurcation is supercritical. On the primary branch, where $A = A_0$ constant, we find $P = \sqrt{1 + cA_0^2}$, and hence from (2.9)

$$q = (\mu - 3A_0^2)\sqrt{1 + cA_0^2}, \tag{2.10}$$

which, on simplifying, yields

$$9cA_0^6 + (9 - 6c\mu)A_0^4 + (c\mu^2 - 6\mu)A_0^2 + \mu^2 - q^2 = 0.$$

To locate the bifurcation points indicating modulational instability we set $A = A_0(1 + ae^{iKX})$. Substituting this ansatz into (2.9) and linearizing in $a$, we obtain

$$0 = (\mu - 4K^2 - 9A_0^2)a - (\mu - 3A_0^2)\frac{1 - 2cA_0^2}{1 + cA_0^2}a,$$

where we have used (2.10) to eliminate $q$. Simplifying further, we find that modulational instability occurs when

$$15cA_0^4 + (6 - 3c\mu + 4cK^2)A_0^2 + 4K^2 = 0.$$

In the limit of large domains, $K = 2\pi/(\varepsilon L) \ll 1$, we therefore expect instabilities when

$$A_0^2 = \frac{4K^2}{3c\mu - 6} + O(K^4) \qquad \text{and} \qquad A_0^2 = \frac{c\mu - 2}{5c} + O(K^2). \tag{2.11}$$

Clearly, no modulational instability is possible if $c\mu < 2$. The first of the conditions in (2.11) indicates that instability occurs at small $A_0$, near the primary bifurcation at $\mu = q$. The second condition indicates that instability also occurs at large amplitudes.

The continuation software AUTO [14] was used to solve (2.9) as a boundary-value problem in a finite domain. Neumann boundary conditions $A_X = A_{XXX} = 0$ at $X = 0, \varepsilon L$ were imposed to avoid numerical difficulties arising from the continuous translational symmetry implied by periodic boundary conditions. Bifurcation diagrams for the supercritical and subcritical cases are shown in Figure 2. Of particular note in Figure 2(b) is that the branch of localized states both extends further into $\mu < q$ than the uniform branch, i.e., $\mu_{sn1} < \mu_{sn2} < q$, and also extends substantially into $\mu > q$ before rejoining the primary branch at large amplitudes.

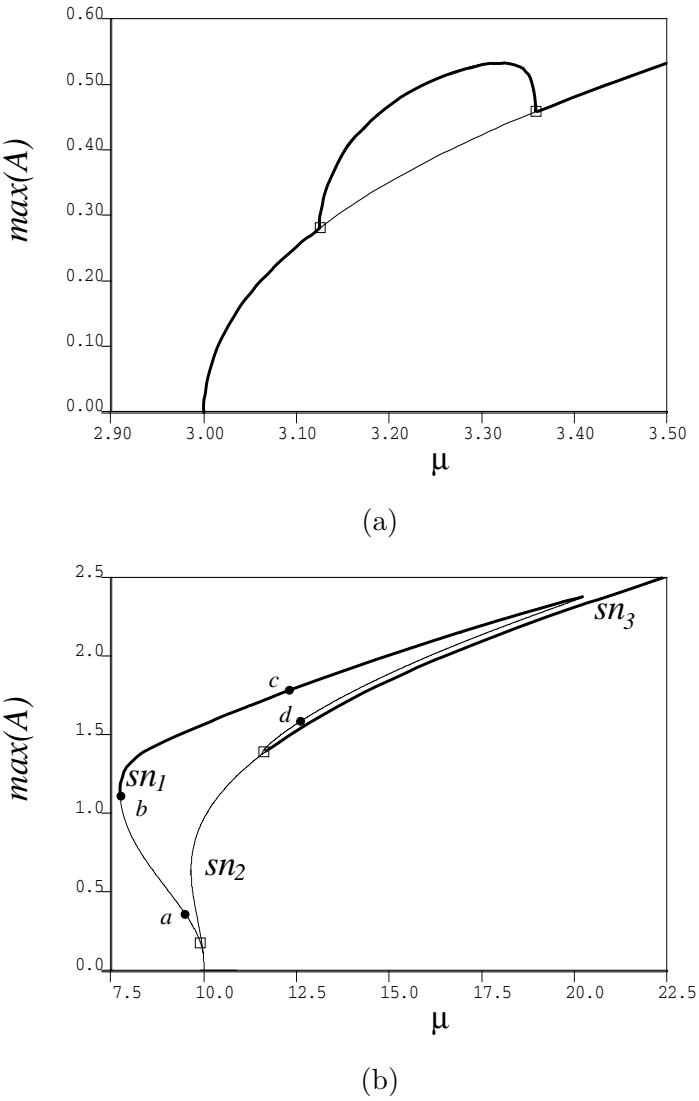


**Figure 2.** *Bifurcation diagrams in the* $(\mu, \max(A))$ *plane. Thick and thin lines denote stable and unstable branches, respectively. A primary branch of uniform amplitude pattern bifurcates from* $A(X) \equiv 0$ *when* $\mu = q$*. We fix* $c = 1$ *and the domain size* $\varepsilon L = 10\pi$*.* $\square$ *denotes bifurcation points from the uniform branch to the branch of modulated states.* (a) $q = 3$*, for which the primary bifurcation is supercritical.* (b) $q = 10$*, for which the primary bifurcation is subcritical. Note in both cases the existence of a secondary instability leading to a branch of spatially localized states. Labels in* (b) *correspond to the different parts of Figure 3.*

Figure 3 shows solutions to (2.9) at the four points indicated on the localized branch in Figure 2(b). Close to the ends of the branch the solution takes on the usual sech-like profile; at the center it resembles a pair of tanh-like fronts between the trivial state $A = 0$ and a nonzero constant value $A_0$. Stable fronts are possible when the two states have the same "energy"; in the standard description of localized states the energies are equal at a single value of the driving parameter $\mu$, known as the "Maxwell point." In the present case we

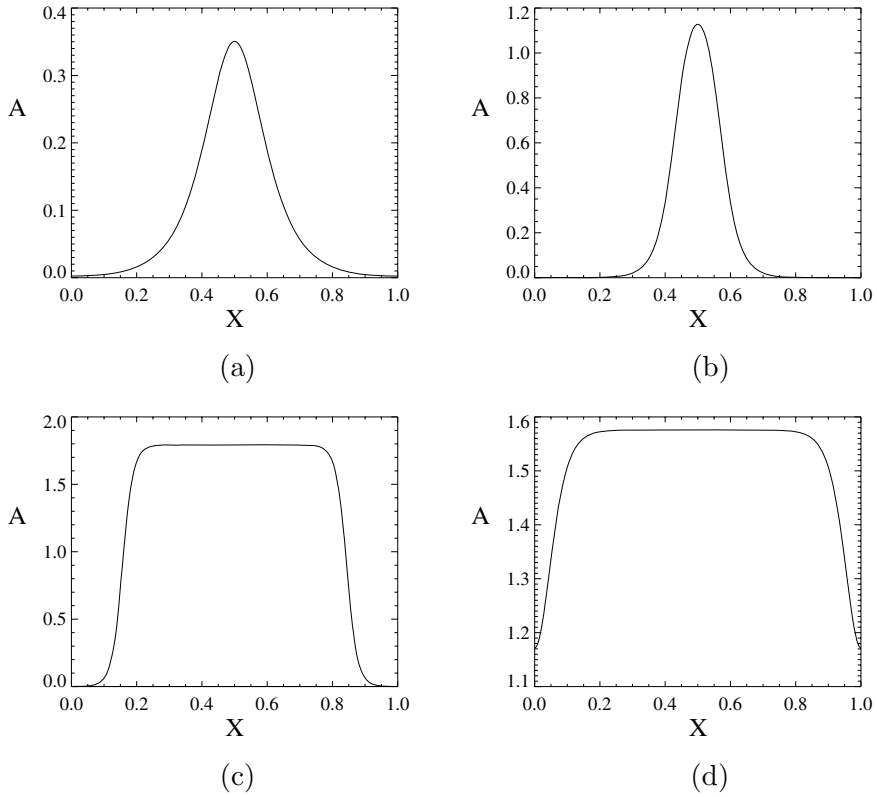


**Figure 3.** *Localized solutions $A(X)$ of (2.9) at the four points on the secondary branch of localized states indicated on Figure 2(b). Parameter values:* (a) $\mu = 9.523$; (b) $\mu = 7.737$; (c) $\mu = 12.373$; (d) $\mu = 12.534$. *Domain size $\varepsilon L = 10\pi$, $c = 1$, $q = 10$. Note that the horizontal axis is rescaled to $[0, 1]$ in the figures.*

expect that the value $A_0$ depends on the driving parameter $\mu$ but not on the domain size or the overall magnitude $q$ of the large-scale mode. These intuitions can be demonstrated with a straightforward, but surprisingly accurate, calculation to estimate the relation between $A_0$ and $\mu$, as we now show.

Equation (2.9) has a first integral, obtained by multiplying by $A_X$ and integrating:

$$E = \frac{\mu}{2}A^2 + 2A_X^2 - \frac{3}{4}A^4 + \frac{qP^2}{c}\frac{1}{\sqrt{1+cA^2}}. \tag{2.12}$$

Assuming that the localized solution resembles Figure 3(c) and is nearly piecewise constant, we may neglect the $A_X$ term in (2.12); this turns out not to affect the accuracy of the following calculation in any significant way, while considerably simplifying the computation. Supposing that the solution is $A = A_0 \neq 0$ over a proportion $\ell/L$ of the domain, and zero on the remainder, from (2.8) we obtain $P = P_\ell$, where

$$\frac{1}{P_\ell} = 1 + \frac{\ell}{L}\left(\frac{1}{\sqrt{1+cA_0^2}} - 1\right). \tag{2.13}$$

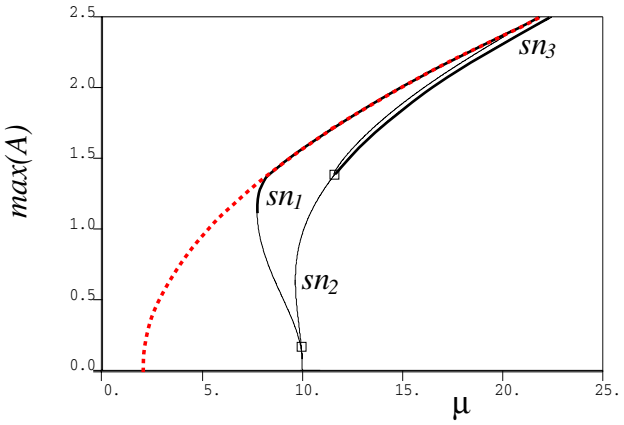


**Figure 4.** *Bifurcation diagram in the* $(\mu, \max(A))$ *plane for* $q = 10$, $c = 1$, $\varepsilon L = 10\pi$, *as in Figure* 2(b). *Thick and thin lines denote stable and unstable branches, respectively.* □ *denotes bifurcation points from the uniform branch to the branch of modulated states. The "Maxwell curve" given by* (2.15) *is the dashed red curve. The central part of the stable branch of localized states is indistinguishable from it.*

Comparing the values of $E$ above and below a front connecting the trivial and nontrivial states in different parts of the domain, we obtain

$$E|_{A=0} = \frac{qP_\ell^2}{c},$$
$$E|_{A=A_0} = \frac{\mu}{2}A_0^2 - \frac{3}{4}A_0^4 + \frac{qP_\ell^2}{c}\frac{1}{\sqrt{1+cA_0^2}},$$

and from (2.9) we also have

$$qP_\ell^2 = (\mu - 3A_0^2)(1+cA_0^2)^{3/2}. \tag{2.14}$$

Equating $E|_{A=0} = E|_{A=A_0}$ and eliminating $qP_\ell^2$ using (2.14), we obtain the following relation between $\mu$ and $A_0$:

$$cA_0^2\left(\mu - \frac{3}{2}A_0^2\right) = 2(\mu - 3A_0^2)(1+cA_0^2)\left(\sqrt{1+cA_0^2} - 1\right).$$

This can be simplified to the cubic polynomial in $A_0^2$:

$$144c^2A_0^6 + (207c - 96c^2\mu)A_0^4 + (72 + 16c^2\mu^2 - 108c\mu)A_0^2 + 12\mu(c\mu - 2) = 0. \tag{2.15}$$

For $\mu = 12$ we find that this analytic result predicts $A_0 = 1.7590818$, compared to the numerical value from (2.9), corresponding to Figure 3(c), of $A_0 = 1.759082$. Moreover, instead of a Maxwell point we have a "Maxwell curve" along which stable fronts, and therefore localized states, exist; see Figure 4. It is worth remarking that (2.15) relates the amplitude $A_0$ only to the linear driving parameter $\mu$ and does not contain the coupling parameter $q$ or the proportion $\ell/L$ of the domain that contains the localized pattern. As a result, the localized pattern

amplitude depends only on $\mu$. This is physically reasonable in the magnetoconvection case: when the magnetic field has been expelled from one part of the fluid domain, the amplitude of the thermal convection that results is due to the thermal driving alone.

Our final remark in this section is that on combining (2.13) and (2.14) we can relate $q$ and $\ell/L$, assuming that $A_0$ is determined from $\mu$ using (2.15):

$$q = (\mu - 3A_0^2)(1 + cA_0^2)^{3/2}\left(1 + \frac{\ell}{L}\left(\frac{1}{\sqrt{1+cA_0^2}} - 1\right)\right)^2.$$

Approximating this expression in the limit of "strong coupling and strong driving," where $q \sim \mu \gg 3A_0^2 \gg 1$, it can be written in the form

$$\frac{q}{\mu} \approx A_0^3\left(1 - \frac{\ell}{L}\right)^2,$$

which is reminiscent of (4.5) in [13] and indicates that in the strong coupling and strong driving regime it is some combination of $q$ and $\mu$ that determines the width of the localized state. Note that the amplitude $A_0$ scales in some unspecified way with $\mu$ and $q$, and so this relation does not indicate a simple power-law scaling exponent, as we discuss further in the next section.

**2.3. Scaling laws in the nonlocal Ginzburg–Landau equation.** The location and shape of the primary and secondary branches evolve continuously between Figures 2(a) and 2(b) as $q$ is increased, first by the introduction of saddle-node points on the secondary branch, and then by the subcriticality of the primary branch. Figure 5 displays the bifurcation structure in the $(\mu, q)$ plane; for $q \gg 10$ the bifurcation points appear to scale as power-laws with increasing $q$, and the region of existence of stable localized states increases in size rapidly. Figure 5 (in which $c = 1$) shows that the localized states exist subcritically (i.e., for $\mu - q < 0$) even for $q < 6$, where the primary bifurcation is still supercritical.

The scaling law for the saddle-node bifurcation $sn_2$ on the uniform amplitude branch can be located by eliminating $A_0^2$ between the second condition of (2.11) and (2.10). This yields the curve

$$\left(cq\frac{5\sqrt{5}}{2}\right)^2 = (3 + c\mu)^3, \tag{2.16}$$

which agrees closely with numerical calculations and is shown as the red dot-dashed curve in Figure 5(b). At large $q$, (2.16) agrees exactly with the numerical results in Figure 5(a).

Fitting the same functional form to the saddle-node curves $sn_1$ and $sn_3$ results in the scaling laws $sn_1$: $q \approx 0.0927(\mu + 3.55)^{1.987}$, $sn_3$: $q \approx 0.298(\mu + 27.9)^{0.986}$ to three significant figures. These exponents are intriguing, and, while they fit the data extremely well at large $q$, they differ significantly from ratios of small integers. It is possible that they can be deduced using the properties of solutions of (2.9) involving the snoidal and cnoidal special functions. At small $q$ we note that there is systematic deviation from power-law scalings.

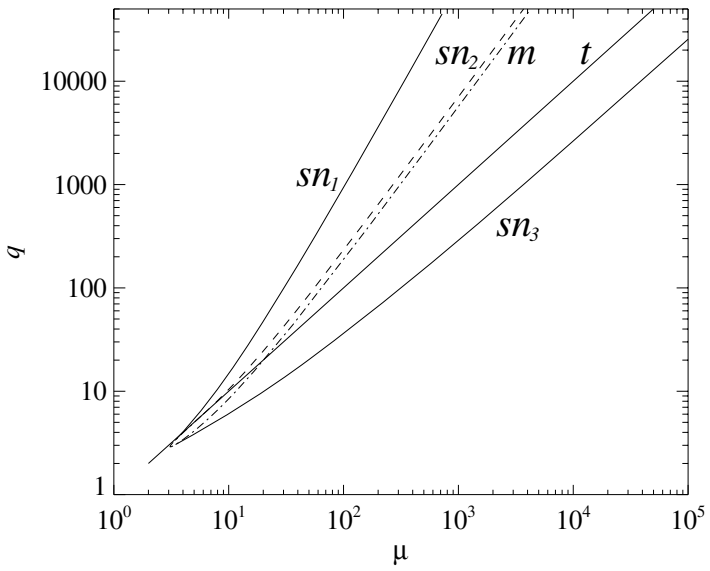


(a)

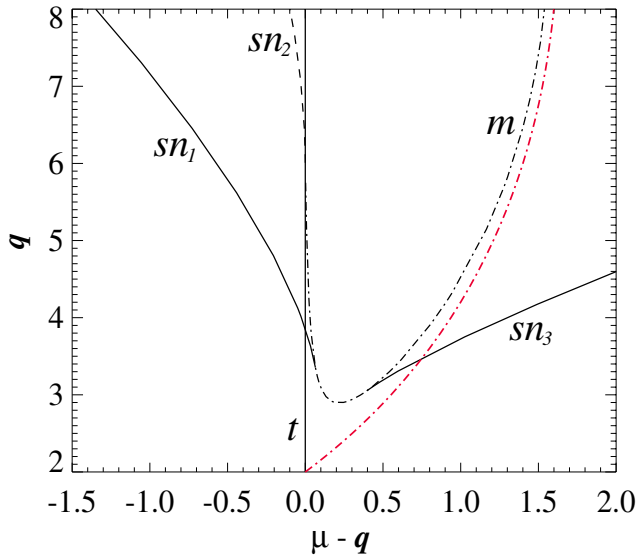


(b)

**Figure 5.** (a) *Bifurcation diagram in the* $(\mu, q)$ *plane showing the power-law behavior of the bifurcation curves at large* $q$. $c = 1$, *domain size* $\varepsilon L = 10\pi$. (b) *Enlargement of* (a) *for small* $q$, *plotted in the* $(\mu - q, q)$ *plane for clarity.* $sn_1$ *and* $sn_3$ *refer to saddle-node bifurcations on the branch of localized states.* $sn_2$ *is the saddle-node on the primary, uniform amplitude branch.* $t$ *refers to the linear instability point* $\mu = q$. $m$ *labels the modulational instability of the primary branch above the saddle-node point, with the red dot-dashed line indicating the analytic result* (2.16).

**3. Numerical results for slanted snaking.** Returning to the Swift–Hohenberg model (2.1)–(2.2), we find, corresponding to the Ginzburg–Landau analysis, that the modulational instability leads to branches of localized states for which the periodic pattern is locked to the modulating envelope. As for the standard snaking scenario, two distinct pairs of branches persist—one pair where the phase difference between pattern and envelope is 0 or $\pi$ and one pair where it is $\pm\pi/2$. The numerical procedure, again using AUTO [14], was as follows.

Starting at the trivial solution $w(x) \equiv 0$, either "Dirichlet" $w(0) = w_{xx}(0) = w(L) = w_{xx}(L) = 0$ or "Neumann" $w_x(0) = w_{xxx}(0) = w_x(L) = w_{xxx}(L) = 0$ boundary conditions were used to avoid the neutral eigenvalue associated with the translational invariance when locating the linear instability at $r = Q$ and switch easily onto the uniform amplitude pattern branch. By continuation along the uniform amplitude branch we located the first modulational instability (indicated by the lower solid square symbol in Figure 6), and AUTO was able to switch onto the modulated branch. We now replace the Dirichlet or Neumann boundary conditions in the numerics with periodic ones, supplemented with a global integral constraint to fix the overall phase of the solution and ensure that there is no drift in the direction of the neutrally stable translation mode. The implementation of the integral constraint followed Rademacher, Sandstede, and Scheel [29]; it was found to be numerically very robust. This approach also accurately detects the "cross-link" or "ladder" branches [5, 22] of asymmetric localized states that complete the bifurcation structure. As in the standard homoclinic snaking scenario, these cross-link branches are never stable; they are omitted from Figure 6 to aid clarity.

Two continuations, one beginning with Dirichlet boundary conditions and one with Neumann boundary conditions, were carried out. The full snaking bifurcation diagram is obtained by superimposing the results. This procedure provides an additional check on the numerical accuracy. Figure 6 indicates that, as expected, these branches are intertwined (around the "Maxwell curve") and stretch both below and above the bifurcation points from the uniform amplitude branch. We call this behavior "slanted snaking." Figure 7 illustrates the evolution of the localized states along the snaking branches.

Another feature of Figure 6 not captured by the Ginzburg–Landau reduction is that the wavelength along the branch of localized states in Figure 6 decreases as $r$ increases; in consequence the branches of localized states terminate on a different uniform amplitude primary branch, in this case one with wavelength $L/8$. This aspect of the bifurcation diagram is brought out clearly in Figure 8, where the vertical axis is $\max(w)$ rather than the $L^2$ norm.

Decreasing $r$ from, say, $r = 3.5$ on the localized branch therefore results in a stepwise decrease in the number of bumps of localized pattern, as the successive saddle-node bifurcations are passed. As $\varepsilon$ decreases the localization becomes increasingly pronounced.

Alternatively we may consider the driving parameter $r$ to be fixed and consider the effect of increasing the strength of the coupling $Q$ between the large-scale field and the pattern mode. For the Ginzburg–Landau system this corresponds to a vertical section through Figure 5(a); the same stepwise series of saddle-node bifurcations is seen in (2.1)–(2.2) when $Q$ is decreased at fixed $r$. Figure 9 (for which $r = 1$) illustrates the location of the lowest two saddle-node bifurcations on the snaking branch as $\varepsilon$ is decreased. Localized states are born in a modulational instability close to $Q = 1$ and exist in $Q > 1$ up to the curve $sn_1$ on which they undergo the first saddle-node bifurcation on the snaking curve. The branch then turns around

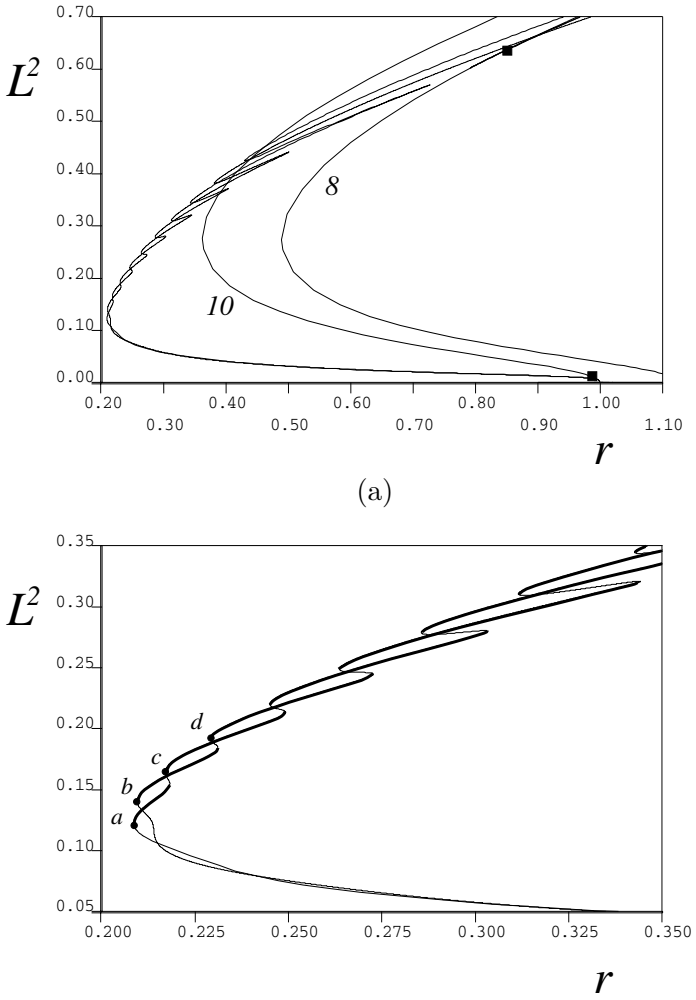


**Figure 6.** *Slanted snaking in* (2.1)–(2.2)*,* $c = Q = 1$*, domain size* $L = 20\pi$*.* (a) *Branches* 10 *and* 8 *denote uniform spatial patterns with wavelengths* $L/10$ *and* $L/8$*, respectively. Snaking branches bifurcate from the* 10 *branch near* $r = 1$ *(at the solid square) and extend down to* $r = 0.21$*. They then continue up to* $r \approx 3.8$ *(not shown) before returning to terminate on the* 8 *branch, indicated by a solid square.* (b) *Enlargement of* (a) *showing the characteristic intertwining of the two snaking branches. Thick and thin lines indicate stable and unstable solutions, respectively. Labels a–d refer to Figure* 7*.*

and continues as $Q$ decreases, up to the second solid line at which the second saddle-node bifurcation on the snaking curve takes place. Subsequent pairs of saddle-node bifurcations are not shown; numerical results indicate that the next pair, and possibly others, rather curiously follows the same power-law scaling with $\varepsilon$ as the first pair. As $\varepsilon$ increases, the region of stable localized states shrinks until it disappears for $\varepsilon > 0.46$. For comparison, Figure 9 also shows the location of the saddle-node bifurcation of the uniform amplitude pattern $sn_2$. The power-law for the curve $sn_2$ follows that derived in (2.16) for the location of the modulational instability near the saddle-node bifurcation $sn_2$: the scaling $q^2 \propto \mu^3$ for large $q$ and $\mu$ implies

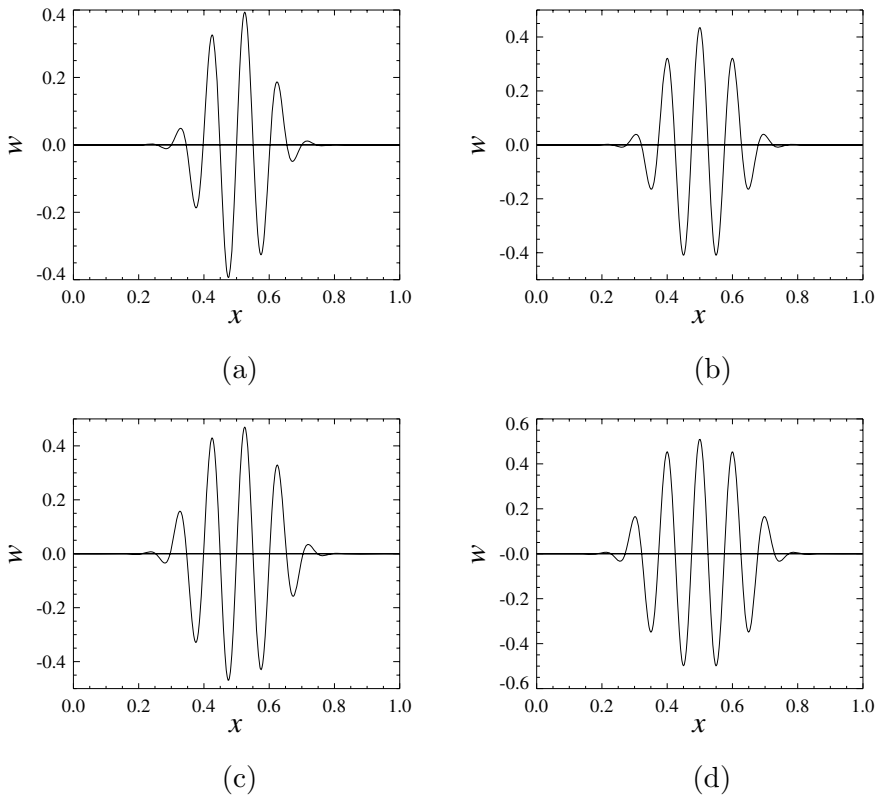


**Figure 7.** *Localized states at four saddle-node bifurcation points in Figure* 6(b). (a) *and* (c) *lie on the* $\phi = \pi/2$ *(odd) branch;* (b) *and* (d) *lie on the* $\phi = 0$ *(even) branch.* $c = Q = 1$*;* $L = 20\pi$*. Note that the domain has been rescaled to* $[0, 1]$.

$(Q/\varepsilon^2)^2 \propto (r/\varepsilon^2)^3$, i.e., $Q \propto \varepsilon^{-1} r^{3/2}$. This scaling agrees with Figure 9.

For $sn_1$ we found in the Ginzburg–Landau approximation (shown in Figure 5) that $q \propto \mu^{1.987}$ for large $q, \mu$. This implies $Q/\varepsilon^2 \propto (r/\varepsilon^2)^{1.987}$, which yields $Q \propto \varepsilon^{-1.974}$. For comparison, Figure 9 indicates the different scaling $Q \propto \varepsilon^{-2.03}$. This difference is too large to be explained purely in terms of numerical errors. We believe that the difference is due to the "beyond-all-orders" terms that determine the width of the homoclinic snaking wiggles in Figure 6 and that are neglected in the multiple-scales analysis of section 2.

For completeness we note that the lower solid line in Figure 9 follows the power-law $Q \propto \varepsilon^{-1.31}$, which has no counterpart in the multiple-scales asymptotics of section 2; clearly the width of the snake, and therefore this power law exponent also, is influenced by the beyond-all-orders asymptotic scalings.

**4. Discussion.** In this paper we have examined a very simple model equation for the influence of a neutrally stable long-wavelength mode on steady-state pattern formation. Such a situation is motivated by several physical problems, and we have fixed on model equations containing symmetries appropriate to the onset of thermal convection in an imposed vertical magnetic field, a long-studied problem in the literature [7, 6, 27].

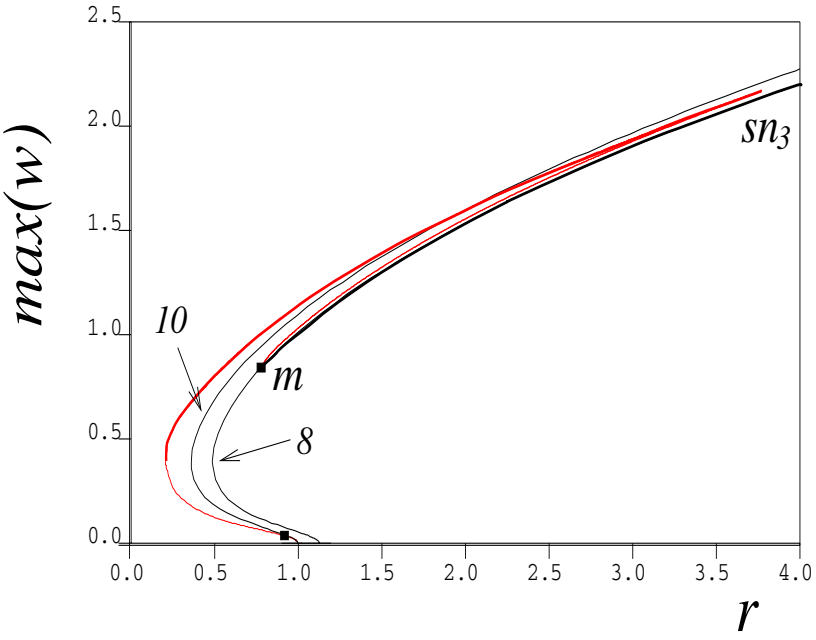


**Figure 8.** *Bifurcation behavior in (2.1)–(2.2) for $c = Q = 1$ and domain size $L = 20\pi$. The bifurcation curves are as for Figure 6; plotting $\max(w)$ against $r$ shows more clearly the excursion of the secondary branch up to $r \approx 3.8$, and the termination of the snaking branches (now superimposed) on the 8 branch. Solid squares denote the bifurcations from uniform periodic patterns to localized patterns. Thick and thin lines denote stable and unstable branches, respectively. Red and black lines denote localized and spatially periodic solution branches, respectively.*

We introduce a new approach to the usual weakly nonlinear multiple-scales analysis, taking the diffusivity of the large-scale mode as the small parameter while allowing order unity fluctuations in amplitude. We then carry out the multiple-scales expansion to third order and deduce a nonlocal Ginzburg–Landau equation that describes the dynamics. It is found that the subcriticality induced by the large-scale mode distorts the usual homoclinic snaking picture and allows localized states to exist over a much larger region of parameter space than is possible in its absence. We refer to this distortion of homoclinic snaking as "slanted snaking." As a result, the existence of a large-scale mode provides a far more robust physical mechanism for the stabilization of localized solutions than the "locking" or "pinning" mechanism that explains their existence in an exponentially small wedge of parameter space in the standard picture.

In other respects the localized states qualitatively resemble standard homoclinic snaking. For example, the secondary branches of asymmetric localized states, found by Burke and Knobloch [5] (called "ladders" in that paper), which link the two snaking branches exist also in this problem, although for clarity we have omitted them from the figures. For the parameter values we investigate in detail ($\varepsilon = 0.1$, $Q = 1$), it is interesting that the lowest saddle-node point on the snake does not correspond to a single isolated period of the pattern. This indicates that our coupling terms, of a simple kind that admit analytic investigation, do

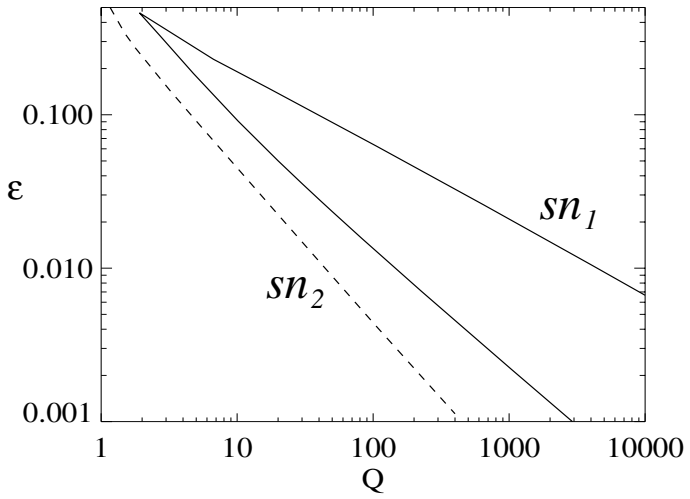


**Figure 9.** *Scaling of the saddle-node bifurcations on the primary and secondary branches of solutions to (2.1)–(2.2) in the $(\varepsilon, Q)$ plane for fixed $r = c = 1$ and domain size $L = 20\pi$. The trivial solution $w(x,t) \equiv 0$ is stable for $Q > 1$. A single localized cell exists between $Q = 1$ and the saddle-node curve $sn_1$; it is stable between the two solid curves. Uniform amplitude states exist (subcritically) below the dashed line $sn_2$.*

not force the pattern to be quite as localized as convection cells appear to be in simulations of the full fluid equations [2, 13]. It is quite possible that more complicated coupled terms, involving extra derivatives of either $B(x,t)$ or $w(x,t)$, deform the snake still further, allowing only a single convection cell to persist at small $r$ or, equivalently, large $Q$. Possible forms for these coupling terms are discussed further in Appendix A.

Overall, these results provide a convincing explanation of the link between homoclinic snaking and the stepwise reduction in the number of cells in the localized states with increasing $Q$ as found first by Blanchflower [3] and reproduced in [13] (see Figure 8 therein). Various features of the full magnetoconvection problem, such as the destabilization of localized steady states by an oscillatory instability in the quiescent region, are, of course, not reproduced by this model. But steady-state features are well reproduced, for example, the evidence, from Figure 9(a) of [13], that the two curves of saddle-node bifurcations that bound the region of the existence of a single-roll localized state scale in different ways with the small parameter $\varepsilon \equiv \zeta$. This is certainly true for the solid lines in Figure 9.

The exponents of the power-law scalings that we present, in both the multiple-scales analysis and the full Swift–Hohenberg model, seem to be strongly dependent on the exact form of the nonlinear coupling terms. A detailed investigation of such dependencies and possible explanations through the properties of analytic solutions in terms of Jacobi elliptic functions are left for future work.

The corresponding calculation for systems for which the large-scale mode is a density is very similar to the analysis presented in detail here. Indeed, the only change required to the model equations is to take the coupling term to be $QBw$ in (2.1). Brief details of the resulting calculations are contained in Appendix B. A further extension is to examine systems where it

appears that the large-scale mode promotes localized activity but the short-scale dynamics is not "pattern-forming." A clear example of this is the vertically and horizontally shaken granular layer experiments of Götzendorfer et al. [17]. In these experiments the vertical excitation of a granular layer does not result in uniform excitation of the material, but rather in a patch of highly energetic particles, while the remainder of the domain remains inactive. Götzendorfer et al. refer to this, slightly fancifully perhaps, as the "sublimation" of the "solid" phase of the material into a "gaseous" form. The general mechanism is, however, physically clear: there is a balance between the (rapid) flux of particles from the active part of the layer into the quiet part as energetic particles are propelled upward and outward, and the natural (slow) trickling of particles from the quiet part back into the active one. These two processes correspond, respectively, to the two terms on the right-hand side of (B.2). Moreover, when the layer height locally exceeds a critical value, the vertical excitation cannot excite particles directly in that part of the bed; this effect is captured by the damping term $Q\rho w$ in (B.1). Model equations capturing exactly these effects were written down by Tsimring and Aranson [32].

There are close connections between this work and that of Matthews and Cox and others [24, 9, 10, 16, 36]; these authors studied systems essentially equivalent to (2.1)–(2.2) obtained by applying $\partial_{xx}^2$ to the right-hand side of the standard Swift–Hohenberg equation (1.1), including both quadratic and cubic nonlinearities in $N(w)$. In these papers the weakly nonlinear analysis proceeds by looking for small distortions of the large-scale mode, i.e., a small parameter $\delta$ and a long lengthscale $X = \delta x$ are introduced, before expanding $w = \delta a(X)\sin x + O(\delta^2)$ and $B = 1 + \delta^2 b(X) + O(\delta^3)$. The resulting amplitude equations for $a(X)$ and $b(X)$ enable the detection of secondary modulational instabilities, as happens here, even in the case that the initial pattern-forming instability is supercritical, which is analogous to Figure 2(a). However, these scalings implicitly restrict our attention only to cases of small disturbances to the distribution of the large-scale mode; the present analysis can, in this sense, go further.

Other physical systems that show related phenomena, and which we intend to examine in future work, include the numerical results of Tsitverblit and Kit [33] on natural double-diffusive convection (see, for example, their Figure 1, which appears to show snaking behavior that does not have the saddle-node points aligned to only two values of the bifurcation parameter). Moreover, model equations for dielectric gas discharge (due to Purwins and collaborators [31, 28]) and for optical cavity lasers [15] have been proposed which include integral terms. These integral terms appear to play the same role in enhancing localization in these systems as the nonlinear diffusion equation for the large-scale mode does in this paper.

**Appendix A. Magnetoconvection.** In this appendix we briefly sketch the derivation of an evolution equation for the large-scale mode in the magnetoconvection case, starting from the governing equations. This justifies the form of our model equation (2.2).

For thermal convection in a vertical magnetic field, the appropriate governing equations for the fluid velocity $\mathbf{u}(x,y,z,t)$, the temperature perturbation $\theta(x,y,z,t)$, and the magnetic field $\mathbf{B}(x,y,z,t)$ are the momentum, temperature, and induction equations:

$$\begin{aligned}\partial_t\mathbf{u} + \mathbf{u}\cdot\nabla\mathbf{u} &= -\nabla p + \sigma R\theta\hat{\mathbf{z}} + \sigma\zeta Q\mathbf{B}\cdot\nabla\mathbf{B} + \sigma\nabla^2\mathbf{u},\\ \partial_t\theta + \mathbf{u}\cdot\nabla\theta &= w + \nabla^2\theta,\\ \partial_t\mathbf{B} &= \nabla\times(\mathbf{u}\times\mathbf{B}) + \zeta\nabla^2\mathbf{B}.\end{aligned}$$

For simplicity we restrict our attention to two-dimensional solutions, ignoring the $y$ coordinate; the extension of these calculations to three dimensions would appear to be straightforward. The temperature variable $\theta(x,z,t)$ is the perturbation to the conduction profile $T = 1 - z$. The velocity and magnetic fields are solenoidal: $\nabla \cdot \mathbf{u} = \nabla \cdot \mathbf{B} = 0$. Note that $\mathbf{B}$ is the full magnetic field—not the perturbation to an initially vertical field of strength unity.

The dimensionless groups are the Rayleigh number $R$, Chandrasekhar number $Q$, Prandtl number $\sigma = \nu/\kappa$, and magnetic Prandtl number $\zeta = \eta/\kappa$.

We suppose that the boundaries are stress-free and are held at fixed temperatures, and we constrain the field to be vertical there. These boundary conditions allow a simple analytical treatment. The linear theory for the onset of thermal convection in a vertical field is well known [7, 27, 10, 13]. We look for small-amplitude solutions in one horizontal dimension, taking $\zeta$ as our small parameter (i.e., $\varepsilon = \zeta$). We propose the solution ansatz

$$\begin{aligned}\mathbf{u} &= (u_1 \cos \pi z, 0, w_1 \sin \pi z),\\ \theta &= \theta_1 \sin \pi z,\\ \mathbf{B} &= (B_x \sin \pi z, 0, B_z \cos \pi z + B_0),\end{aligned}$$

where $u_1$, $w_1$, $B_x$, $B_z$, and $B_0$ are functions of $x$ and $t$ only. Computing $\hat{\mathbf{z}} \cdot \nabla \times (\mathbf{u} \times \mathbf{B})$ we obtain equations for the $z$ independent terms and, separately, those that depend on $\cos \pi z$:

$$\partial_t B_0 = \frac{1}{2}(w_1 B_x - u_1 B_z)' + \zeta B_0'', \tag{A.1}$$

$$\partial_t B_z = -(u_1 B_0)' + \zeta(B_z'' - \pi^2 B_z), \tag{A.2}$$

where primes $'$ denote $\partial_x$. We assume that the quantities $u_1, w_1, B_x, B_z$ all vary on a short spatial scale with wavenumber $k$, so that we may, at leading order, replace $\partial_{xx}^2 \to -k^2$, where it acts on these variables. As a result the solenoidal conditions $\nabla \cdot \mathbf{u} = 0$ and $\nabla \cdot \mathbf{B} = 0$ imply $u_1 = \pi/k^2 \partial_x w_1$ and $B_x = -\pi/k^2 B_z$, which allows us to eliminate $u_1$ and $B_x$ from (A.1)–(A.2). We obtain

$$\partial_t B_0 = -\frac{\pi}{2k^2}(w_1 B_z)'' + \zeta B_0'', \tag{A.3}$$

$$\partial_t B_z = -\frac{\pi}{k^2}(w_1' B_0)' + \zeta(B_z'' - \pi^2 B_z). \tag{A.4}$$

Since the linear eigenfunction for the onset of weakly nonlinear convection involves $u_1$, $w_1$, $B_x$, and $B_z$, it is clear also that $B_z$ does not evolve independently of $w_1$. Looking for steady states of (A.4), we expect, therefore, that $B_z = -\pi/(k^2\beta^2\zeta)(w_1' B_0)'$ near onset, where $\beta^2 = k^2 + \pi^2$. Substituting this into (A.3) yields an evolution equation for the large-scale field $B_0(x,t)$, coupling it to the weakly nonlinear convection pattern amplitude $w_1(x,t)$:

$$\partial_t B_0 = \frac{\pi^2}{2k^4\beta^2\zeta}\left(w_1(w_1' B_0)'\right)'' + \zeta B_0''.$$

This is of the same form as (2.2), setting $c = \pi^2/(2k^4\beta^2)$, except for two extra derivatives in the first term. Since near onset $w_1$ involves only the single lengthscale $2\pi/k$, and $B_0 \approx 1$, it is clear that these derivatives will not qualitatively change the behavior. However, it is quite

possible that they will alter the exponents of various scaling laws, for example, those shown in Figure 9. A similar evaluation of the $\hat{\mathbf{z}}$ component of the $\mathbf{B}\cdot\nabla\mathbf{B}$ term, and subsequent use of the above approximations of $B_x$ and $B_z$ in terms of $B_0$ and $w_1$, yield, heuristically, the term that couples the large-scale mode back to the vertical velocity:

$$\partial_t w_1 = \cdots + \frac{\sigma Q\pi^2}{k^2\beta^2}\left(\frac{B_0'}{k^2}+B_0\right)(w_1'B_0)'.$$

**Appendix B. A density-like large-scale mode.** Suppose that a one-dimensional pattern-forming system is described by the pattern amplitude $w(x,t)$ and a density-like large-scale mode $\rho(x,t)$, for example, the local layer height in a granular medium or thin film. In this case the symmetry $\rho\to-\rho$ is absent, and the corresponding model equations are

$$w_t = [r-(1+\partial_{xx}^2)^2]w - w^3 - Q\rho w, \tag{B.1}$$

$$\rho_t = \varepsilon\rho_{xx} + \frac{c}{\varepsilon}(\rho w^2)_{xx}. \tag{B.2}$$

As before, we set $\frac{1}{L}\int_0^L \rho(x,t)dx \equiv \langle\rho\rangle = 1$. We restrict our attention to steady solutions, setting $\partial_t\equiv 0$, and integrate (B.2) twice to obtain

$$\rho = \frac{P}{1+cw^2/\varepsilon^2}, \qquad \text{where} \qquad \frac{1}{P}\equiv\left\langle\frac{1}{1+cw^2/\varepsilon^2}\right\rangle_x. \tag{B.3}$$

Substituting this into (B.1) and looking for steady states, we find

$$0 = [r-(1+\partial_{xx}^2)^2]w - w^3 - \frac{QPw}{1+cw^2/\varepsilon^2}.$$

We now introduce the multiple-scales ansatz $w(x,t) = \varepsilon A(X)\sin x + \varepsilon^2 w_2 + \varepsilon^3 w_3 + \cdots$, introducing the long lengthscale $X=\varepsilon x$. We rescale the parameters $r=\varepsilon^2\mu$ and $Q=\varepsilon^2 q$ in the standard way. At third order in the expansion an amplitude equation for $A(X)$ is obtained by multiplying by $\sin x$ and integrating over the short lengthscale, denoting the average $\frac{1}{2\pi}\int_0^{2\pi}\cdot\,dx \equiv \langle\,\cdot\,\rangle$. This yields

$$0 = \mu A + 4A_{XX} - 3A^3 - 2qP\left\langle\frac{A\sin^2 x}{1+cA^2\sin^2 x}\right\rangle_x, \tag{B.4}$$

where the constant $P$ is defined as before:

$$\frac{1}{P} = \frac{1}{\varepsilon L}\int_0^{\varepsilon L}\frac{1}{2\pi}\int_0^{2\pi}\frac{1}{1+cA^2\sin^2 x}\,dx\,dX \equiv \left\langle\left\langle\frac{1}{1+cA^2\sin^2 x}\right\rangle_x\right\rangle_X = \left\langle\frac{1}{\sqrt{1+cA^2}}\right\rangle_X.$$

Carrying out the $x$-integral in (B.4), we obtain

$$0 = \mu A + 4A_{XX} - 3A^3 - \frac{2qP(\sqrt{1+cA^2}-1)}{cA\sqrt{1+cA^2}}. \tag{B.5}$$

Consideration of the last term in the limit $A \to 0$ indicates that there is no singularity at small $A$ and that the trivial solution $A = 0$ is linearly unstable when $\mu > q$.

It can be seen that (B.5) has a first integral,

$$E = \frac{\mu}{2} + 2(A_X)^2 - \frac{3}{4}A^4 - \frac{2qP}{c}\left[\log A + \tanh^{-1}\left(\frac{1}{\sqrt{1+cA^2}}\right)\right],$$

in which, after some manipulation, the last term on the right-hand side can be rewritten to give

$$E = \frac{\mu}{2} + 2(A_X)^2 - \frac{3}{4}A^4 - \frac{qP}{c}\log F(A),$$

where $F(A) = A^2 + \frac{2}{c}\left[1 + \left(cA^2+1\right)^{1/2}\right]$. We may also eliminate $qP$ to yield the expression corresponding to (2.15) that describes the amplitude of a localized state as a function of $\mu$:

$$(\mu - 3A_0^2)\sqrt{1+cA_0^2}\left[\frac{1}{2}\log F(A_0) - \log\frac{2}{\sqrt{c}}\right] = \left(\frac{\mu}{2} - \frac{3A_0^2}{4}\right)\left(\sqrt{1+cA_0^2} - 1\right).$$

Despite the more complicated functional form, this curve is qualitatively very similar to that defined by (2.15) and provides an analytic estimate of the "Maxwell curve" in this case.

**Acknowledgments.** I would like to acknowledge constructive suggestions from the referees. This work has benefited from instructive and useful conversations with Alan Champneys, Steve Cox, Paul Matthews, and Mike Proctor. It was begun at the Isaac Newton Institute, Cambridge.

## REFERENCES

[1] N. Akhmediev and A. Ankiewicz, eds., *Dissipative Solitons*, Lecture Notes in Phys. 661, Springer-Verlag, Berlin, 2005.
[2] S. M. Blanchflower, *Magnetohydrodynamic convectons*, Phys. Lett. A, 261 (1999), pp. 74–81.
[3] S. M. Blanchflower, *Modelling Photospheric Magnetoconvection*, Ph.D. thesis, University of Cambridge, Cambridge, UK, 1999.
[4] A. Bose and G. A. Kriegsmann, *Stability of localized structures in non-local reaction-diffusion equations*, Methods Appl. Anal., 5 (1998), pp. 351–366.
[5] J. Burke and E. Knobloch, *Localized states in the generalized Swift–Hohenberg equation*, Phys. Rev. E (3), 73 (2006), 056211.
[6] F. H. Busse, *Nonlinear interaction of magnetic field and convection*, J. Fluid Mech., 71 (1975), pp. 193–206.
[7] S. Chandrasekhar, *Hydrodynamic and Hydromagnetic Stability*, Clarendon, Oxford, UK, 1961; republished by Dover, New York, 1981.
[8] P. Coullet, C. Riera, and C. Tresser, *Stable static localized structures in one dimension*, Phys. Rev. Lett., 84 (2000), pp. 3069–3072.
[9] S. M. Cox and P. C. Matthews, *Instability and localisation of patterns due to a conserved quantity*, Phys. D, 175 (2003), pp. 196–219.
[10] S. M. Cox, P. C. Matthews, and S. L. Pollicott, *Swift–Hohenberg model for magnetoconvection*, Phys. Rev. E (3), 69 (2004), 066314.
[11] M. C. Cross and P. C. Hohenberg, *Pattern formation outside of equilibrium*, Rev. Modern Phys., 65 (1993), pp. 851–1112.
[12] F. A. Davidson and N. Dodds, *Spectral properties of non-local differential operators*, Appl. Anal., 85 (2006), pp. 717–734.

[13] J. H. P. Dawes, *Localized states in thermal convection with an imposed vertical magnetic field*, J. Fluid Mech., 570 (2007), pp. 385–406.
[14] E. Doedel, A. R. Champneys, T. Fairgrieve, Y. Kuznetsov, B. Sandstede, and X. Wang, *AUTO97: Continuation and Bifurcation Software for Ordinary Differential Equations*, 1997, http://indy.cs.concordia.ca/auto/.
[15] W. J. Firth, L. Columbo, and A. J. Scroggie, *Proposed resolution of theory-experiment discrepancy in homoclinic snaking*, Phys. Rev. Lett., 99 (2007), 104503.
[16] A. A. Golovin, S. H. Davis, and P. W. Voorhees, *Self-organisation of quantum dots in epitaxially strained solid films*, Phys. Rev. E (3), 68 (2003), 056203.
[17] A. Götzendorfer, J. Kreft, C. A. Kruelle, and I. Rehberg, *Sublimation of a vibrated granular monolayer: Coexistence of gas and solid*, Phys. Rev. Lett., 95 (2005), 135704.
[18] Y. Hiraoka and T. Ogawa, *Rigorous numerics for localized patterns to the quintic Swift–Hohenberg equation*, Japan J. Indust. Appl. Math., 22 (2005), pp. 57–75.
[19] R. B. Hoyle, *Pattern Formation: An Introduction to Methods*, Cambridge University Press, Cambridge, UK, 2006.
[20] G. W. Hunt, M. A. Peletier, A. R. Champneys, P. D. Woods, M. A. Wadee, C. J. Budd, and G. J. Lord, *Cellular buckling in long structures*, Nonlinear Dynam., 21 (2000), pp. 3–29.
[21] G. Iooss and M. C. Pérouème, *Perturbed homoclinic solutions in reversible* 1 : 1 *resonance vector fields*, J. Differential Equations, 102 (1993), pp. 62–88.
[22] G. Kozyreff and S. J. Chapman, *Asymptotics of large bound states of localized structures*, Phys. Rev. Lett., 97 (2006), 044502.
[23] C. R. Laing, W. C. Troy, B. Gutkin, and G. B. Ermentrout, *Multiple bumps in a neuronal model of working memory*, SIAM J. Appl. Math., 63 (2002), pp. 62–97.
[24] P. C. Matthews and S. M. Cox, *Pattern formation with a conservation law*, Nonlinearity, 13 (2000), pp. 1293–1320.
[25] L. M. Pismen, *Patterns and Interfaces in Dissipative Dynamics*, Springer Ser. Synergetics 15, Springer-Verlag, Berlin, 2006.
[26] Y. Pomeau, *Front motion, metastability and subcritical bifurcations in hydrodynamics*, Phys. D, 23 (1986), pp. 3–11.
[27] M. R. E. Proctor and N. O. Weiss, *Magnetoconvection*, Rep. Progr. Phys., 45 (1982), pp. 1317–1379.
[28] H.-G. Purwins, H. U. Bödeker, and A. W. Liehr, *Dissipative solitons in reaction-diffusion systems*, in Dissipative Solitons, Lecture Notes in Phys. 661, Springer-Verlag, Berlin, 2005, pp. 267–308.
[29] J. D. M. Rademacher, B. Sandstede, and A. Scheel, *Computing absolute and essential spectra using continuation*, Phys. D, 229 (2007), pp. 166–183.
[30] H. Sakaguchi and H. R. Brand, *Stable localized solutions of arbitrary length for the quintic Swift–Hohenberg equation*, Phys. D, 97 (1996), pp. 274–285.
[31] C. Strümpel, H.-G. Purwins, and Y. A. Astrov, *Spatiotemporal filamentary patterns in a dc-driven planar gas discharge system*, Phys. Rev. E (3), 63 (2001), 026409.
[32] L. S. Tsimring and I. S. Aranson, *Localized and cellular patterns in a vibrated granular layer*, Phys. Rev. Lett., 79 (1997), pp. 213–216.
[33] N. Tsitverblit and E. Kit, *The multiplicity of steady flows in confined double-diffusive convection with lateral heating*, Phys. Fluids A, 5 (1993), pp. 1062–1064.
[34] P. B. Umbanhowar, F. Melo, and H. L. Swinney, *Localized excitations in a vertically vibrated granular layer*, Nature, 382 (1996), pp. 793–796.
[35] A. G. Vladimirov, J. M. McSloy, D. V. Skryabin, and W. J. Firth, *Two-dimensional clusters of solitary structures in driven optical cavities*, Phys. Rev. E (3), 65 (2002), 046606.
[36] D. M. Winterbottom, P. C. Matthews, and S. M. Cox, *Pattern formation in a model of a vibrated granular layer*, SIAM J. Appl. Dynam. Systems, 7 (2008), pp. 63–78.
[37] P. D. Woods and A. R. Champneys, *Heteroclinic tangles and homoclinic snaking in the unfolding of a degenerate reversible Hamiltonian–Hopf bifurcation*, Phys. D, 129 (1999), pp. 147–170.